Geomechanics and Engineering, *Vol. 11, No. 4 (2016) 587-605*
DOI: http://dx.doi.org/10.12989/gae.2016.11.4.587

Determination of tunnel support pressure under the pile tip using upper and lower bounds with a superimposed approach

Yong-Joo Lee*

Department of Civil Engineering, Seoul National University of Science and Technology, 232 Gongneung-ro, Nowon-gu, Seoul 139-743, Republic of Korea

(*Received November 16, 2015, Revised May 18, 2016, Accepted June 08, 2016*)

Abstract. This study aimed to develop upper and lower bounds to predict the tunnel support pressure under the pile tip during the circular tunnel excavation. Most previous studies on the upper and lower bound methods were carried out for the single ground structures, e.g., retaining wall, foundation, ground anchor and tunnel, in the homogeneous ground conditions, since the pile-soil-tunnel interaction problem is very complicated and sophisticated to solve using those bound methods. Therefore, in the lower bound approach two appropriate stress fields were proposed for single pile and tunnel respectively, and then they were superimposed. In addition, based on the superimposition several failure mechanisms were proposed for the upper bound solution. Finally, these upper bound mechanisms were examined by shear strain data from the laboratory model test and numerical analysis using finite element method.

Keywords: pile-soil-tunnel interaction; upper and lower bounds; tunnel support pressure; stress field; superimposition; upper bound mechanism; shear strain

1. Introduction

One procedure for developing the possible failure mechanism for a tunnelling pressure problem is to consider the stress discontinuities adopted for a "lower bound" approach and to couple these with the slip characteristic directions in the zones between the stress discontinuities. If the best lower bound solution and the best upper bound mechanistic solution correspond and provide an identical answer, this solution is acceptable as satisfying both equilibrium and kinematic compatibility and does not violate failure criterion. In contrast to the above tunnel pressure most previous studies focused on the ground movements, surface settlements and tunnel behaviour associated with the tunnelling operations so far (Goh and Hefney 2010, Wang *et al*. 2010, Do *et al*. 2014, Mazek 2014).

In relation to the upper and lower bound methods several previous studies were carried out for the single ground structures only, e.g., retaining wall, foundation, ground anchor and tunnel etc., in the homogeneous ground conditions (Chen 1975, Atkinson and Potts 1977, Davis *et al*. 1980, Atkinson 1981, Leca and Dormieux 1990, Kame *et al*. 2012). In addition, Sloan and Assadi (1993) carried out stability analysis of shallow tunnels in soft ground using the finite element formulation

*Corresponding author, Associate Professor, E-mail: ucesyjl@seoultech.ac.kr

http://www.techno-press.org/?journal=gae&subpage=7 ISSN: 2005-307X (Print), 2092-6219 (Online)

of those two bound methods. Recently, basic bound solution concepts for ϕ' soil were introduced to assess the ultimate bearing capacity of an embedded wall by Lee (2006). Subsequently, Lee (2007) has done assessment of tunnel collapse load by upper and lower bound approaches with FE analysis. Recently, collapse mechanism of deep tunnel considering effects of seepage forces in layered soil was derived using a new curved failure mechanism based on the framework of upper bound theorem (Yang and Yan 2015).

Bound calculations are relevant to homogeneous, isotropic materials as plastic failure is developed. Lower bounds are based on equilibrium across assumed “stress discontinuities” and Mohr’s circle is used to determine the stress changes. Upper bounds incorporate a complete kinematically admissible rupture mechanism. The best answers are obtained when the rupture mechanisms and the stress discontinuity pattern are common (Lee 2004).

In this paper, the author presents several upper bound mechanisms together with a lower bound solution to obtain the tunnel support pressure, P_0 for the pile-soil-tunnel interaction, as shown in Fig. 1. From Fig. 1 a row of loaded piles are assumed to be wall for the plane-strain condition, and soil is considered as frictional dry material, i.e., no cohesion (c = 0). Obviously, there is an interactive zone between the pile tip and the tunnel crown.

The author used the deformation patterns, the shear strain contours and the principal strain and stress directions from the physical model tests and FEA data to assist in his choice of stress fields for lower bound solution and for possible kinematically admissible mechanisms with which to develop the upper bound solutions.

In this paper, first of all an assumed stress field in the lower bound is proposed for single pile and tunnel respectively, and then together with two stress fields they are superimposed to obtain the lower bound solution for the pile-tunnel interaction problem. In addition, based on the superimposed stress field a number of appropriate mechanisms can be derived for the upper bound solution. Finally, tunnel pressures from these upper bound mechanisms are compared to the lower bound solution. In terms of theory the best (or reasonable) upper bound solution should be close to the lower bound solution. Subsequently, shear strain data from the laboratory model test using the close range photogrammetry and numerical analysis using finite element method are also compared with the best upper bound mechanism.

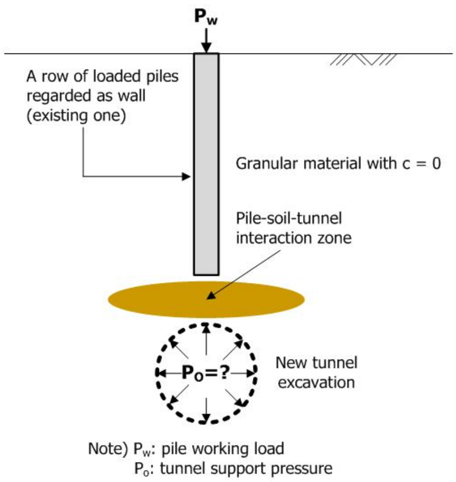

Fig. 1 Tunnelling position below the pile tip for plane-strain condition

2. Basic bound solution concepts for ϕ' material

2.1 Lower bound

For the author's tests on a granular material, the control is the critical state friction angle, ϕ'_{cs} shown by the limiting stress envelope in Fig. 2(a). Where, S' (= $(\sigma'_1 + \sigma'_3) / 2$) is effective mean normal stress and t (= $(\sigma'_1 - \sigma'_3) / 2$) is shear stress. A stress discontinuity will separate two stress states with one common plane across which equilibrium is maintained resulting in a common stress state point C, as shown in Fig. 2(b). ρ' is defined as the angle of mobilised friction on this common plane or discontinuity. The change in principal stress direction across the discontinuity is $\theta_B - \theta_A = \delta\theta$ as also shown in Fig. 2(b). In Fig. 2(c), the line ρ' cuts circle O_A at C_1 and circle O_B at C_2 by geometry. $O_B - C_2$ is parallel to $O_A - C_1$, therefore $\angle XO_BC_2$ is equal to $2\theta_A$ (i.e., $\angle O_BO_AC_1$). As $\angle XO_BC_1$ is $2\theta_B$ then $\angle C_1O_BC_2 = 2\theta_B - 2\theta_A = 2\delta\theta$. If O_BD is set at 90° to OC_1C_2 then $\angle C_1O_BD = \angle C_2O_BD = \delta\theta$. O_BD can be expressed in terms of S'_B and ρ' and of t_B and $\delta\theta$

$$O_BD = S'_B \sin\rho' = t_B \cos\delta\theta \tag{1}$$

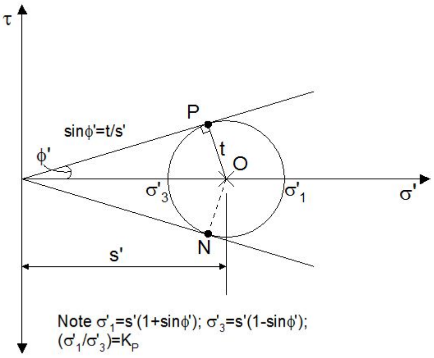

(a) Mohr circle of stress with a limiting envelope for ϕ' material

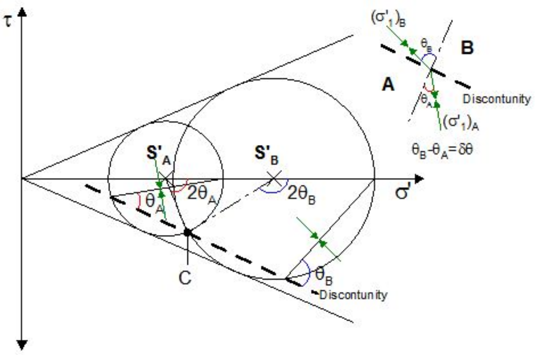

(b) Two stress states with discontinuity and a common point (C)

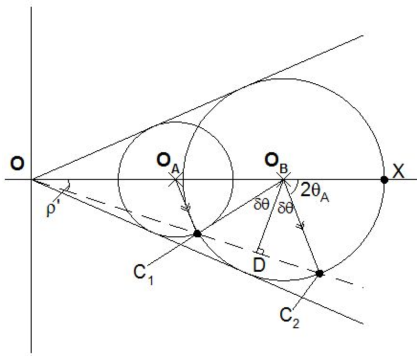

(c) Relationship between ρ' and $\delta\theta$ in Mohr circles

Fig. 2 A limiting stress envelope; discontinuity; common point (C); ρ'; and $\delta\theta$ in association with Mohr circles

Thus, ρ' can be determined as below

$$\sin\rho' = \sin\phi' \cos\delta\theta \tag{2}$$

From the angles $\angle O_B C_2 C_1$ (i.e., $\angle P = 90° - \delta\theta$) and ρ′ as shown in Fig. 3(a), they give $\angle O_B O_A C_1 = P + \rho'$ and $\angle O_A O_B C_1 = P - \rho'$. Therefore, $2\theta_A = P + \rho' = 90° + \rho' - \delta\theta$ and $2\theta_B = 180° - (P - \rho') = 90° + \rho' + \delta\theta$. These angles (i.e., θ_A and θ_B) can be rewritten as below

$$\theta_A = (45^\circ + \frac{\rho'}{2}) - \frac{\delta\theta}{2} \tag{3}$$

$$\theta_B = (45^\circ + \frac{\rho'}{2}) + \frac{\delta\theta}{2} \tag{4}$$

The geometry associated with both θ_A and θ_B angles above, is shown in Fig. 3(b). The distance between $O_A - O_B$ represents the change in S'_A to S'_B, as shown in Fig. 3(c). The stress ratios, i.e., $\frac{t_B}{t_A}$ and $\frac{S'_B}{S'_A}$ can be expressed as below

$$\frac{t_B}{t_A} = \frac{\sin(P+\rho')}{\sin(P-\rho')} = \frac{S'_B}{S'_A} \tag{5}$$

as $P = 90° - \delta\theta$, the above Eq. (5) can be rewritten as below

$$\frac{S'_B}{S'_A} = \frac{\cos(\delta\theta - \rho')}{\cos(\delta\theta + \rho')} \tag{6}$$

if $S'_B - S'_A = \Delta S'$, we can obtain Eq. (7) as below

$$2\sin\delta\theta \sin\rho' = \frac{\Delta S'}{S'}\{\cos\delta\theta\cos\rho' - \sin\delta\theta\sin\rho'\} \tag{7}$$

For very small changes in $\delta\theta$ across a discontinuity such as $\delta\theta \to 0$; $\cos\delta\theta \to 1$; $\sin\delta\theta \to d\theta \to 0$; $2\sin\delta\theta \to 2d\theta$; $\rho' \to \phi'$, the above Eq. (7) can be rewritten as below

$$2d\theta \tan\phi' = \frac{dS'}{S'} \tag{8}$$

for a whole sequence of small angle changes the discontinuities will form a fan. This will change the principal stress direction, $\Delta\theta$ provided

$$2\tan\phi' \int_0^{\Delta\theta} d\theta = \int_{S_A}^{S_B} \frac{1}{S'} dS' \tag{9}$$

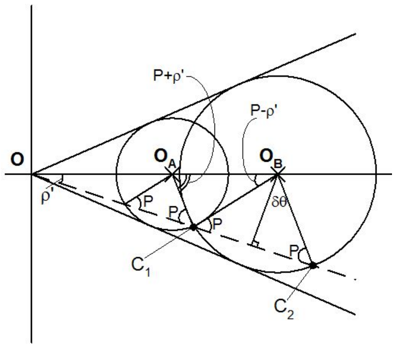

(a) Calculation of θ_A and θ_B based on ρ' and $\delta\theta$

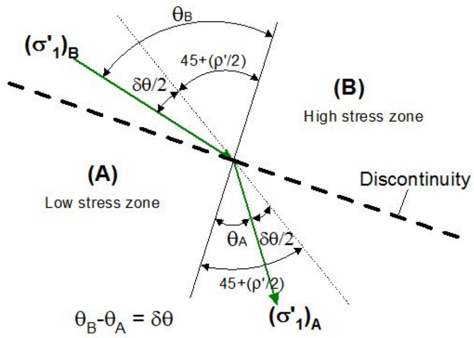

(b) Discontinuity with σ_1 directions

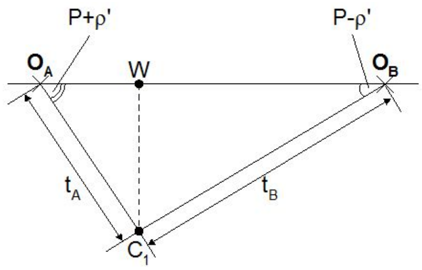

(c) Geometry of S'_A and S'_B with t_A and t_B

Fig. 3 σ'_1 directions associated with ρ' and $\delta\theta$ and geometry of stress ratio (t and S')

giving Eq. (10) below

$$\exp^{2\Delta\theta\tan\phi'} = \frac{S'_B}{S'_A} \tag{10}$$

In order to be able to draw acceptable fields based on straight lines rather than the log spiral above, the author chose to generate stress characteristic lines (α and β), based on a $\delta\theta$ of 15° and for a ϕ' of 26°. These were chosen to provide simple whole angles when using $\frac{\delta\theta}{2}$ and $\frac{\rho'}{2}$. The reason should be clear in Table 1 below. The mobilised friction angle (ρ') and the angles of major principal stress (σ_1) direction (θ_A and θ_B) were calculated, giving the values of ρ'; θ_A and θ_B as shown and from Eq. (6) the stress ratio change should be $\frac{S'_B}{S'_A} = 1.3$.

Table 1 Parameters for stress characteristic lines

ϕ'	ρ'	θ_A $\left(45° + \frac{\rho'}{2} - \frac{\delta\theta}{2}\right)$	θ_B $\left(45° + \frac{\rho'}{2} + \frac{\delta\theta}{2}\right)$
26°	25°	50°	65°

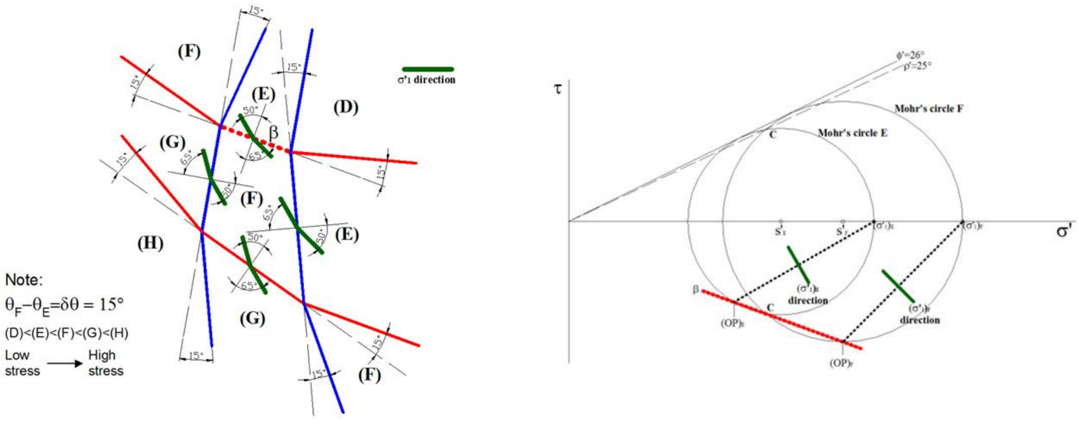

(a) Stress characteristic lines with ϕ' = 26° and $\delta\theta$ = 15°

(b) Mohr circles with stress discontinuity (β) for E and F

Fig. 4 Stress characteristic lines related to Mohr circles

Both α (positive, blue line) and β (negative, red line) stress discontinuity planes for a succession of zones are shown in Fig. 4(a). The β (dotted red line) stress discontinuity (between E and F) cuts Mohr circles E and F at point C, as shown in Fig. 4(b).

2.2 Upper bound

To obtain the upper bound solution in this study, four key assumptions are summarised as below:

(1) The material is permeable and drains. The water is, therefore, not involved in any displacements. In the author's case, the whole experiment is dry.

(2) The granular soil dilates at failure on the "obliquity (ϕ' or ρ')" planes, as shown in Fig. 5(a). The corner of the element moves from the point a to a' as the shear occurs giving rise to the angle of dilation, ψ'. To maintain coincidence of principal axes (i.e., σ_1 and ε_1 directions are the same), normality is assumed for the material behaviour resulting in the angle of ψ' being equal to ϕ', as shown in Fig. 5(b). This assumption is known to be incorrect for granular material. No soil has ever been known to dilate at more than 22° to 25° whereas ϕ' is usually much greater than 30°. However, in an upper bound approach any assumption made will only influence the accuracy. It is known that if the mechanism chosen is closely associated with the best stress field, the error will be minimised. The author's assumption of $\delta\theta$ = 15° and the approach above provides an acceptable upper bound.

(3) Upper bounds involve an assessment of internal work for the virtual work calculation. This involves work done on the shear plane. The relationship between the normal force, N and the shear force, T, is associated by ϕ' giving a resultant force, R, as shown in Fig. 5(c). The dilation, ψ' away from the line of the shear plane means the movement shown in Fig. 5(d). If ψ' = ϕ' then the resulting force, R and the displacement are at right angles to each other (see Fig. 5(e)). Hence, no internal work is done by R. This

means that no internal work is done on failure or shear planes. This is obviously an extreme situation, but the result is of course considerable displacements of the external forces which form the remaining component of the virtual work balance. The large movement of the displaced resulting forces compensates for the elimination of internal work.

(4) In relation to the rupture fan mechanism, the ruptures are formed of two sets governed by the zero extension line directions (see Fig. 6(a)). These are separated by the angle of 90° + ψ'. The rupture plane o-*a*-*b*-*n* is a smooth curve through the fan field for a small angle change (i.e., $\delta\theta$) in the fan. The α rupture will curve through the same angle. As the plane a-b must be at 90° + ψ' to the radius *b*-*P*, for a small angle of $\delta\theta$ the radius *P*-*b* becomes $R + \delta R$ and the length *a*-*x* is $Rd\theta$. Therefore

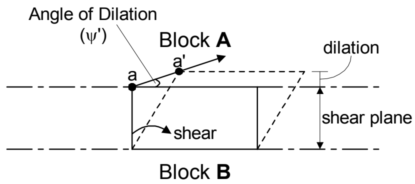

(a) Rupture system

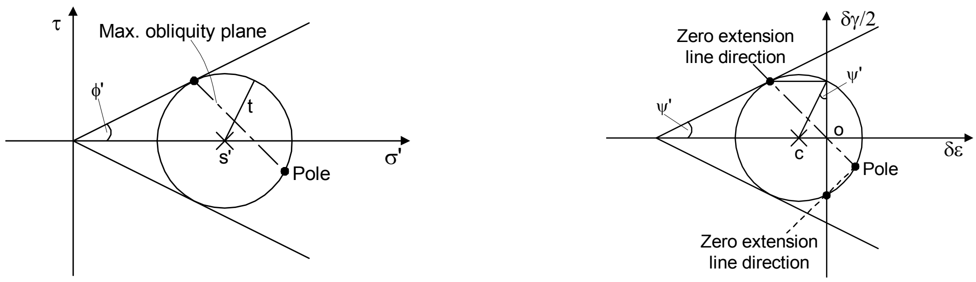

(b) Mohr circles related to Maximum obliquity planes

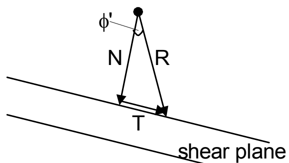

(c) Relation between *N* and *T*

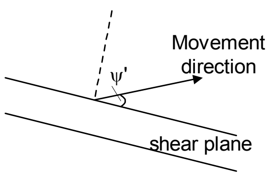

(d) Movement direction with ψ'

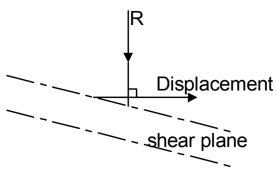

(e) Relation between *R* and displacement

Fig. 5 Fundamental requirements for ϕ' material in the upper bound

$$\frac{dR}{Rd\theta} = \tan\psi' \quad \text{or} \quad \frac{1dR}{R} = \tan\psi' d\theta \tag{11}$$

and then integrating below Eq. (12)

$$\log_e [R]_{R_A}^{R_B} = [\theta \tan\psi'] \tag{12}$$

The radius changes can be expressed as Eq. (13)

$$\frac{R_A}{R_B} = \exp^{\theta_{AB}\tan\psi'} \tag{13}$$

If ψ' is equal to ϕ', the equation of a log spiral can be expressed as

$$\frac{R_A}{R_B} = \exp^{\Delta\theta\tan\phi'} \tag{14}$$

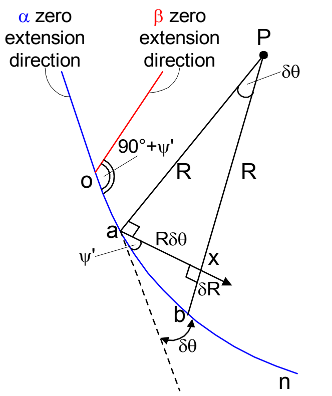

(a) Zero extension line directions

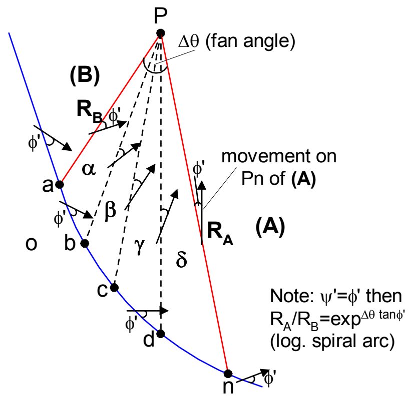

(b) Logarithmic spiral fan system

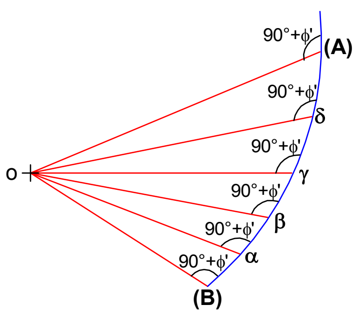

(c) Displacement diagram for a log spiral fan mechanism

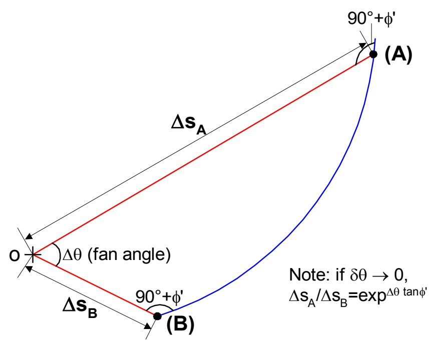

(d) Identical displacement diagram of log spiral

Fig. 6 Physical logarithmic spiral fan mechanism for ϕ' material in the upper bound where $\Delta\theta$ is a full fan angle (see Fig. 6(b)).

If ψ' is equal to 0 (i.e., no dilation; no volume change; undrained conditions), the radius ratio, R_A/R_B is equal to 1. This means that the shape is a circle as shown in Fig. 6(a). Fig. 6(c) shows the displacement diagram associated with the physical failure fan in relation to Fig. 6(b). If $\delta\theta$ is very small (i.e., $\delta\theta \to 0$), the displacement diagram will be an identical type of log spiral, as shown in Fig. 6(d).

3. Stress fields for single pile and tunnel

3.1 Single pile

As an alternative, in order to satisfy $\delta\theta = 15°$ (change of σ'_1 rotation from high stress zone to low stress zone), $\Delta\theta$ of the single stress fan from the stress zone A to B is set to 189° ($\Delta\theta = 189°$) and the length of embedded pile is set to 370 mm from the ground surface with its width of 25 mm (Fig. 7). It is noted that the interface friction angle between the pile and surrounding soil was assumed to be δw = 13°. The stress situation in zone A against the side of the pile is as described by the Mohr circle of stress, as shown in Fig. 8. This gives rise to a principal stress direction at 9° as shown. From zone *B* below the pile σ'_1 therefore rotates 189°. The author has drawn $\delta\theta = 15°$ zones from 0 to 180° and a single 9° zone to the side friction area *B*. The extended stress characteristic lines from Fig. 7 are shown in Fig. 9. These will be used with the tunnel characteristic lines for the pile-soil-tunnel interaction later (see Section 4).

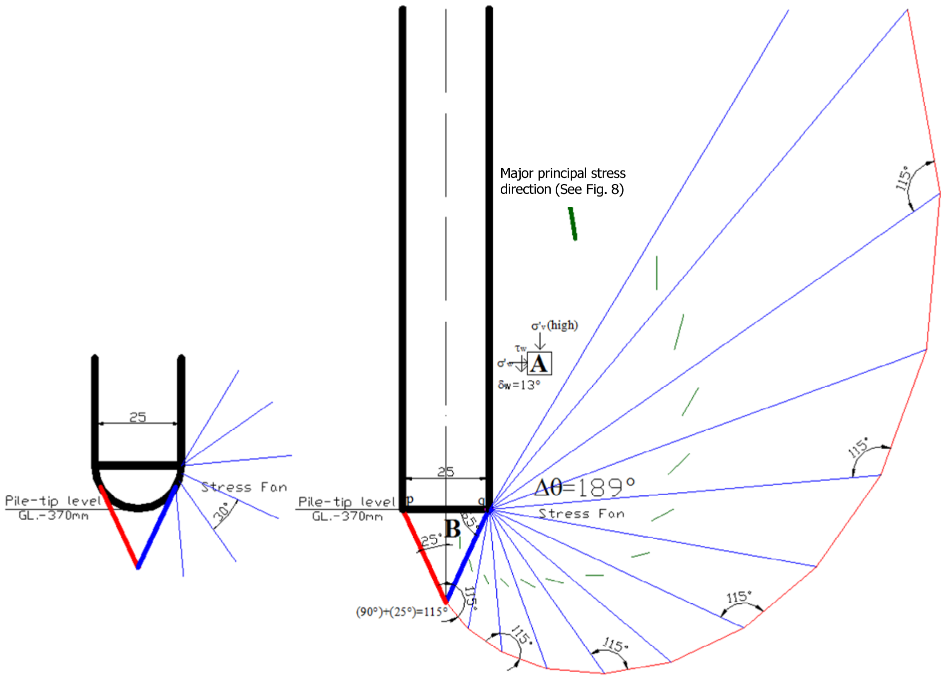

Fig. 7 Stress fan with logarithmic spiral fan, Δθ=189°

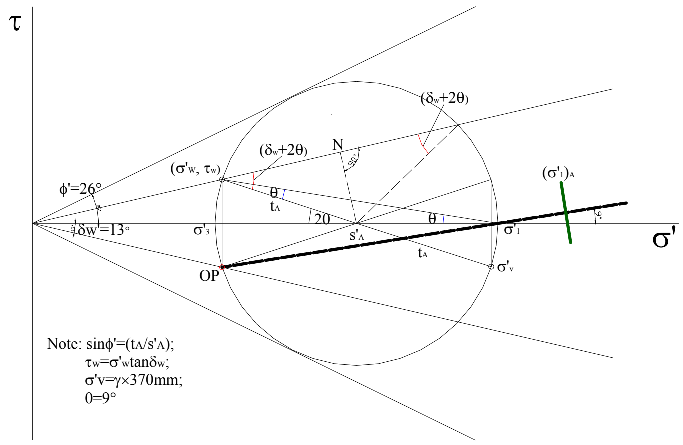

Fig. 8 Mohr's circle of stress in the low stress zone *A* at the pile side

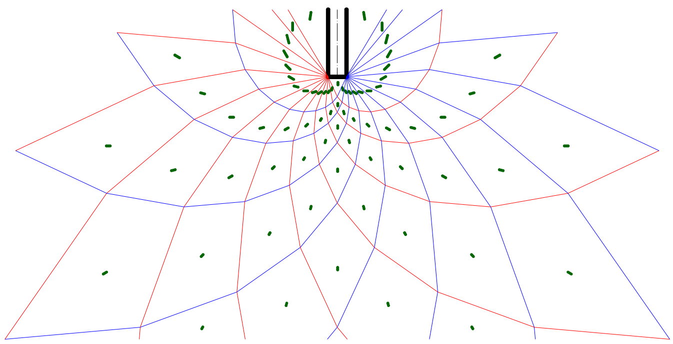

Fig. 9 Postulated α and β stress characteristic lines with σ'_1 directions for the pile-soil-tunnel interaction

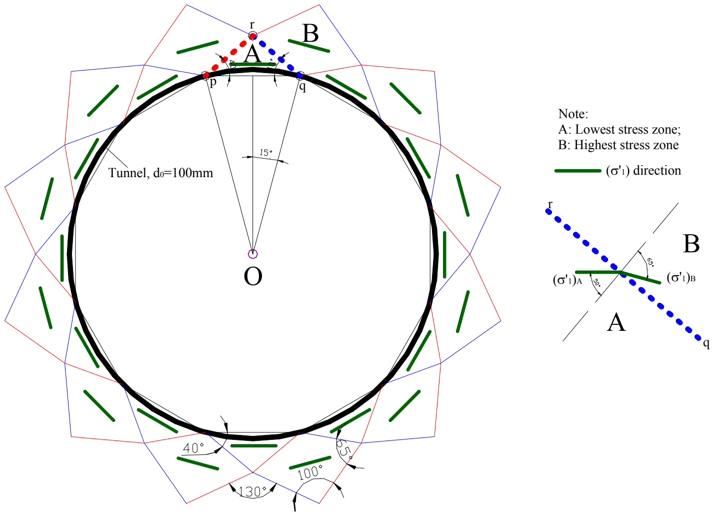

Fig. 10 Stress characteristic lines in association with $\phi' = 26°$ and $\delta\theta = 15°$ for the tunnel

3.2 Tunnel

Fig. 10 shows the two stress discontinuities α (+, blue) and β (-, red) for a material with ϕ' = 26° and $\delta\theta$ = 15°. The tunnel diameter (d_0) is set to 100 mm. Mohr's circles of stress for typical zones A and B are shown in Fig. 11. The two discontinuity lines together with the major principal stress directions are shown. The fully developed diagram of discontinuities around the tunnel is drawn to scale in Fig. 12. The resulting circumferential arrangement of principal stress σ'_1 directions was as observed in both the model test and the FEA data (Lee 2004).

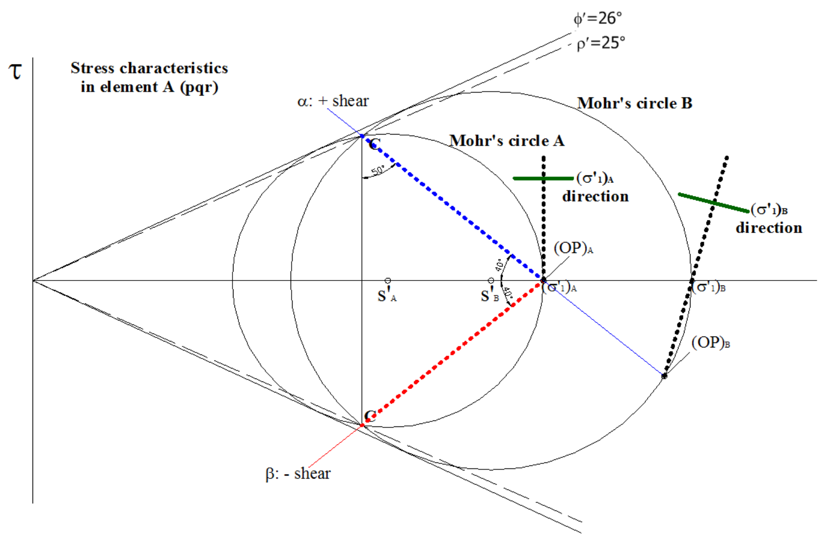

Fig. 11 Mohr circles with stress characteristic lines in the zone *A*

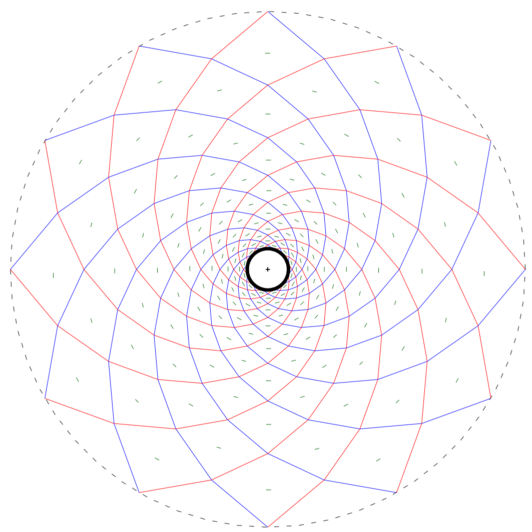

Fig. 12 Postulated α and β stress characteristic lines with σ_1 directions for the tunnel

4. Pile-soil-tunnel interaction

4.1 Introduction

It might appear unusual to consider the established classic upper and lower bound approach for the pile-soil-tunnel interaction situation at this late stage. The problem is a complex interactive one and the availability of both the numerical and the model strain data provided key insights into the possible locations of stress discontinuities and into the potential shapes of failure mechanisms and the resulting rotations of the principal stress directions.

The author had adopted the technique of superimposing the two independent 15° slip line fields onto each other identifying the area in which coincidence of principal stress directions occurs, then taking the relevant α slip line characteristics from the pile tip to the coincidental area from the single pile and then on from there to the tunnel invert area using the independent tunnel case. The number of stress drops along the key characteristics provided a lower bound relationship between the pile tip and the tunnel wall. Combining this key α characteristic with the isotropic zone and a similar key β characteristic to the tunnel crown, a possible mechanism of soil blocks was developed and assuming a fully associated flow rule an upper bound assessment was then made.

4.2 Closed form upper and lower bound approach

In order to calculate the tunnel pressure, P_0 for the lower bound the stress characteristic lines for the single pile proposed above (Fig. 9) are superimposed on the stress characteristic lines for

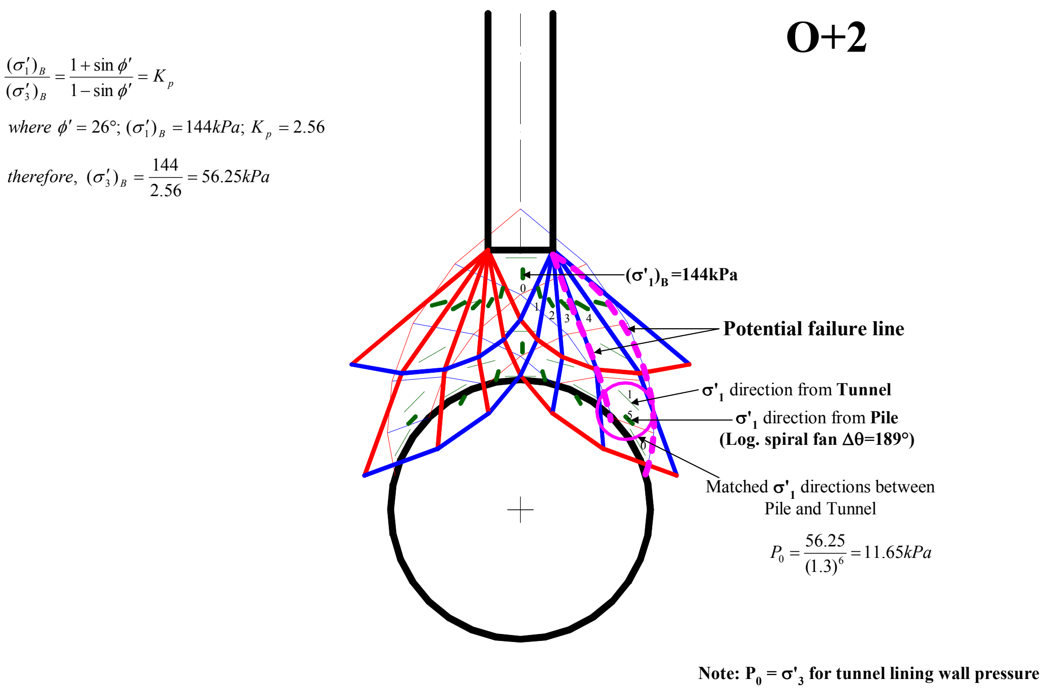

Fig. 13 Lower bound solution for *O*+2

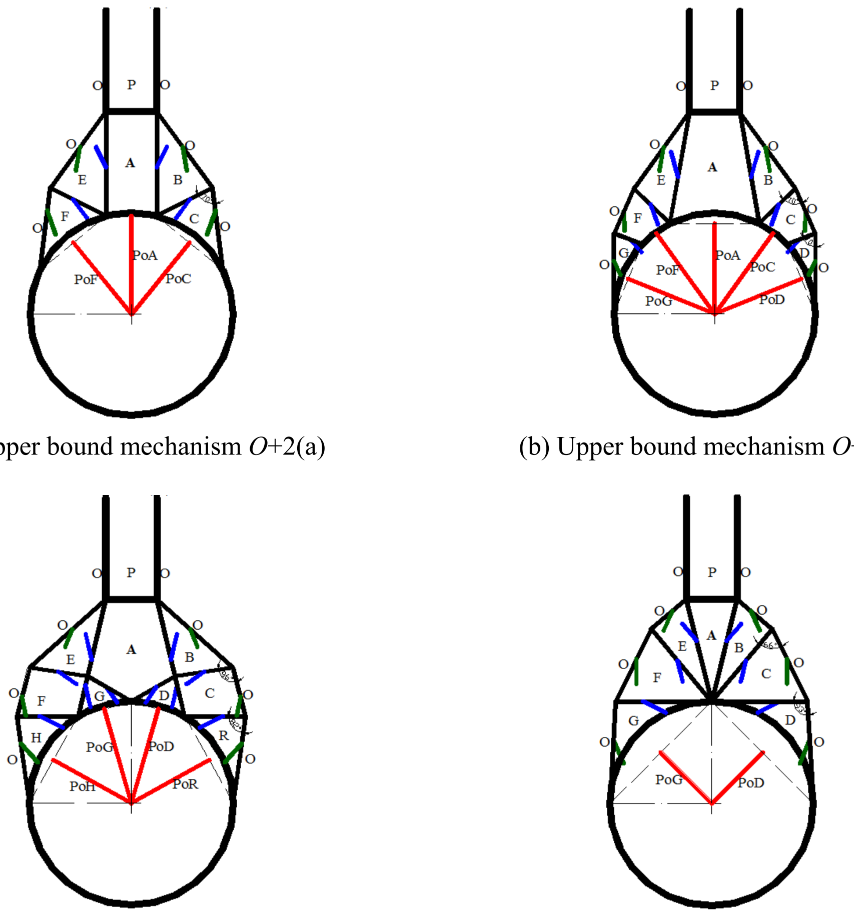

(a) Upper bound mechanism O+2(a)

(b) Upper bound mechanism O+2(b)

(c) Upper bound mechanism O+2(c)

(d) Upper bound mechanism O+2(d)

Fig. 14 Upper bound mechanisms for O+2

the single tunnel (Fig. 12). For the superimposition a case of O+2 was considered in this study, i.e., tunnel is located just below the pile tip (the offset distance from the tunnel centre to the pile tip is one times the tunnel diameter).

The matching principal stress direction occurs in the solid circular area (σ'_1 direction from the tunnel = σ'_1 direction from the pile). There are 5 stress drops from the pile tip and a further 1 stress drops to the tunnel crown from this circular area. Consequently, a total of 6 stress discontinuities appear to be involved with the lower bound calculation, i.e., there are 6 stress discontinuities finishing at the same physical level. Therefore, the value of P_0 at the tunnel crown level will be Eq. (15).

$$P_0 = \frac{K_A(\sigma'_1)_B}{\left(S'_B / S'_A\right)^n} = \frac{K_A(\sigma'_1)_B}{(1.3)^6} = \frac{(\sigma'_3)_B}{(1.3)^6} = 11.65\ kPa \tag{15}$$

Where n is a total number of stress drops (see Fig. 13).

It is noted that the tunnel lining wall pressure, P_0 equals to σ'_3. From Fig. 13 the dotted shear

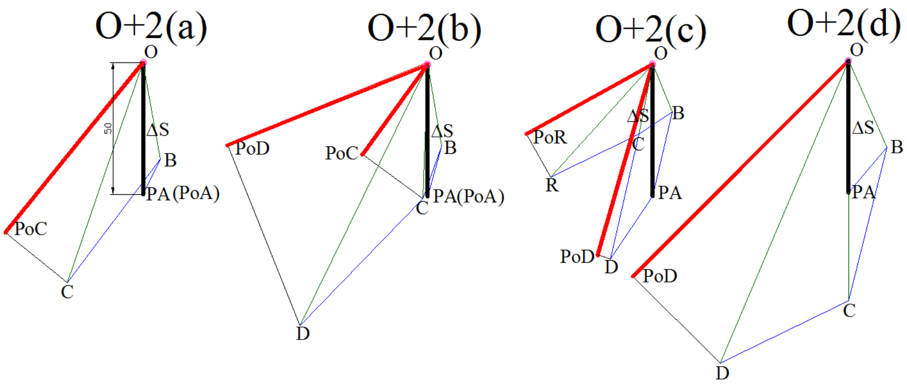

Fig. 15 Corresponding displacement diagrams for O+2

Table 2 Tunnel pressure according to the upper bound mechanisms

Mechanism	O+2(a)	O+2(b)	O+2(c)	O+2(d)
Tunnel pressure, P_0 (kPa)	27.6	39.1	50.7	16.1

band made by the two potential failure lines represents the combined path and was used to develop the upper bound mechanism consisting of several blocks.

The author postulated 4 admissible upper bound mechanisms as shown in Fig. 14. In addition, corresponding displacement diagrams are also presented in Fig. 15. It is noted that right sides of all the mechanisms are considered in the corresponding displacement diagrams due to the symmetric condition.

Table 2 shows tunnel pressure, P_0. Among them, the lowest tunnel pressure, P_0 (= 16.1 kPa) was calculated by the upper bound mechanism O+2(d) (see Figs. 14(d) and 15(d)). The detailed calculation procedure is presented in Appendix.

In terms of theory the best (or reasonable) upper bound solution should be close to the lower bound solution. For this reason the best upper bound mechanism might be O+2(d). This mechanism will be compared to maximum shear strain contours from both the model test and FEA. The purpose of this comparison is looking for the dotted shear band in the lower bound solution shown in Fig. 13 as well as the upper bound mechanism of O+2 shown in Fig. 14(d).

Two features are interesting to note. The first is that between the pile tip and the near side of the tunnel there is a band across which the principal strain direction (ε_1) flips 90°. This band probably represents a zone of isotropic conditions. The α slip characteristic dominates the mechanisms below this band between the pile tip and the tunnel invert while the β characteristic dominates another component of the developing mechanism above the isotropic band between the pile shaft and the tunnel crown. In a mechanism, the isotropic material will be moved as a non-deformed block between these two shear systems. The second feature to note is that close to the pile tip and the shaft, the stress and zero extension directions match the single pile case while close to the tunnel the principal stresses remain close to the circumferential pattern of the single tunnel. The interaction between tunnel and pile clearly links at the points where the principal stress direction from each independent system coincided. If the coincidence spreads over a considerable area, the mechanism will easily form.

Table 3 Material parameters used in the FEA

Material	c (kPa)	ν	ϕ' (°)	ψ (°)	E_0 (MPa)	m_E* (MPa/m)	A (m^2)	γ_{bulk} (kN/m^3)	K_0
Tunnel	-	0.2	-	-	15500	-	0.003	-	-
Soil	0.1	0.35	26	15	1.6	10	-	24	0.66

Note: *based on the Gibson's soil; c: cohesion; ν: Poisson's ratio; ϕ': angle of shearing resistance; ψ: dilation angle; E_0: Young's modulus at reference level; γ_{bulk}: bulk unit weight of soil; K_0: earth pressure coefficient at rest; A: cross sectional area for 2-noded bar element

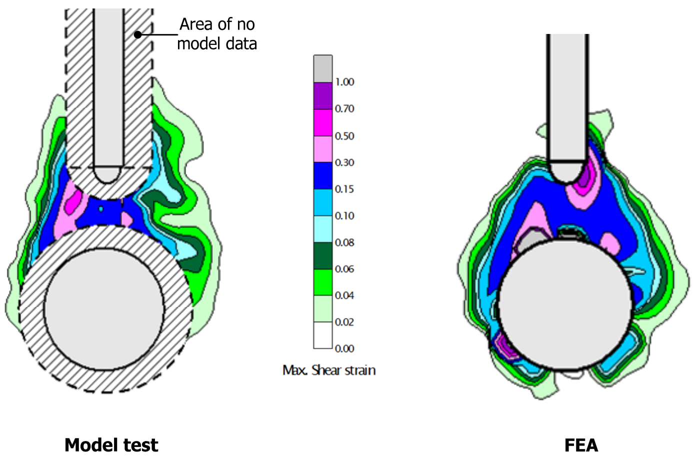

(a) V_L = 10.94%

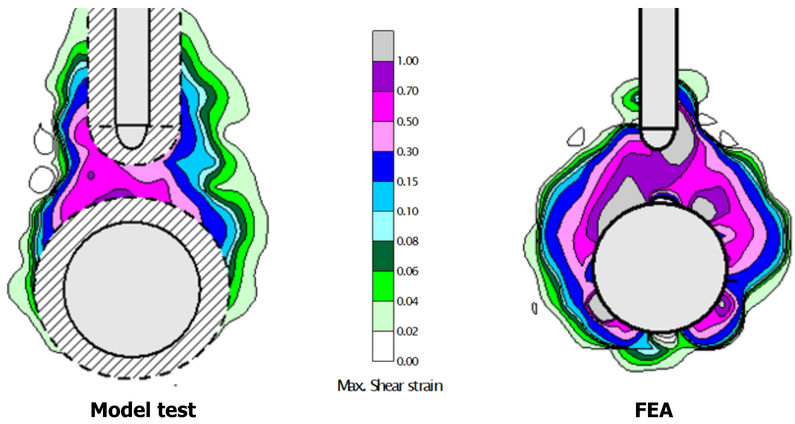

(b) V_L = 18.65%

Fig. 16 Maximum shear strain (γ_{max}) contours at large volume loss

4.3 Comparison between model test and FEA data

In order to check the feasibility of the upper bound mechanism O+2(d), maximum shear strain (γ_{max}) data from both model test and FEA are presented at relatively large volume loss of tunnel (V_L = 10.94% and V_L = 18.65%), as shown in Fig. 16. Mohr-Coulomb model was used to represent soil behaviour and a bar model was adopted for the tunnel boundary system. Table 3 shows material properties used in the FE analysis.

It is noted that values of those volume loss lead to tunnel failure and in order to obtain clear failure mechanisms for the upper bound solution the tunnel volume loss should be bigger than 5% in reality. This is only due to the academic interest. However, in tunnel practice the volume loss should be controlled as low as possible for the safety, i.e., less than 5% in granular material and it depends on the soil conditions (Attewell *et al*. 1986). In addition, more detailed information of model test and FEA can be found in Lee (2004). In this study, the author mainly focuses on both the upper and lower bounds with the superimposition method for the pile-soil-tunnel interaction problem.

From the above comparison it is found that the shear band in the lower bound is well matched with the shear strain distribution from both the model test and FEA. In addition, the upper bound mechanism of *O*+2 consisting of several blocks is similar to the shear strain distribution. As expect the superimposition approach in the lower bound may provide the most reasonable upper bound mechanism which is in consistency of the shear strain distribution.

Fig. 17 shows the P_0 values obtained from FEA data for the critical element adjacent to the tunnel against increasing volume loss. Also, shown are the author's two bound solutions. The stresses from the FEA data show an asymptotic pattern during developing volume loss, which fall very close to the band defined by the bound solutions. For the critical element above the tunnel crown the FE stresses are closer to the lower bound solution at relatively large volume loss.

It is noticed that the tunnel support pressure obtained by the FEA data lies between the upper and lower bounds at volume losses greater than 14%. These volume loss values are relatively large and do not occur in reality as they lead to tunnel failure (as stated before). However, at small

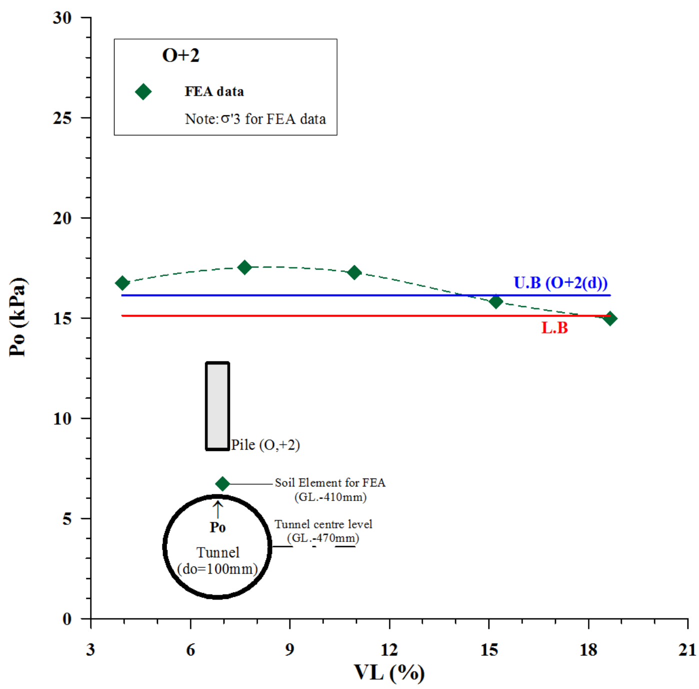

Fig. 17 Comparison between closed form bound solutions and FEA data for *O*+2

volume loss values (approaching 5%) which occur in tunnel practice so that the support pressure approaches only the upper bound not the lower bound.

The author was impressed that the values given by the bound approaches were so comparable with the stresses from the FEA data. In addition, FE values greater than the LB were expected as critical FE elements were not on the tunnel surface, but at least one layer of element into the soil mass.

5. Conclusions

A superimposition method for predicting tunnel support pressure under the pile tip has been proposed in this study.

- The assessment of the single pile and an independent tunnel by upper and lower bound plastic failure analysis proved quite difficult, particularly regarding the influence of the side area of the deep pile and along the vertical axis of the tunnel, between the ground surface and the tunnel crown, where the self-weight influence was only approximately allowed for.
- These restrictions, however, did not significantly influence the patterns of the stress discontinuities and rupture planes below the pile tip and in the zones of either side of the tunnel centre line. These areas formed the zones relevant to pile-soil-tunnel interaction.
- The resulting combination of the two independent bound solutions has given a very acceptable method of assessing the pile-soil-tunnel interaction situation, and the resulting mechanisms agree well with the shear mechanisms indicated by both the FE analysis and the physical model test.
- In the small volume loss (less than 5%), the upper bound approach gives more accurate results of tunnel support pressure than that of the lower bound.

References

Atkinson, J.H. (1981), *Foundations and Slopes*, McGraw-Hill, UK.

Atkinson, J.H. and Potts, D.M. (1977), "Stability of a shallow circular tunnel in cohesionless soil", *Géotechnique*, **27**(2), 203-215.

Attewell, P.B., Yeates, J. and Selby, A.R. (1986), *Soil Movements Induced by Tunnelling and their Effects on Pipelines and Structures*, Blackie, Glasgow, Scotland.

Chen, W.F. (1975), *Limit Analysis and Plasticity*, Elsvier, New York, NY, USA.

Davis, E.H., Gunn, M.J., Mair, R.J. and Seneviratne, H.N. (1980), "The stability of shallow tunnels and underground openings in cohesive material", *Géotechnique*, **30**(4), 397-416.

Do, N.A., Dias, D., Oreste, P. and Maigre, I.D. (2014), "2D numerical investigations of twin tunnel interaction", *Geomech. Eng.*, *Int. J.*, **6**(3), 263-275.

Goh, A.T.C. and Hefney, A.M. (2010), "Reliability assessment of EPB tunnel-related settlement", *Geomech. Eng.*, *Int. J.*, **2**(1), 57-69.

Kame, G.S., Dewaikar, D.M. and Choudhury, D. (2012), "Pullout capacity of vertical plate anchors in cohesion-less soil", *Geomech. Eng.*, *Int. J.*, **4**(2), 105-120.

Leca, E. and Dormieux, L. (1990), "Upper and lower bound solutions for the face stability of shallow circular tunnels in frictional material", *Géotechnique*, **40**(4), 581-605.

Lee, Y.J. (2004), "Tunnelling adjacent to a row of loaded piles", Ph.D. Dissertation; University College London, London, UK.

Lee, Y.J. (2006), "Assessment of ultimate bearing capacity for an embedded wall by closed-form analytical

solution", *J. KGS*, **22**(9), 23-36.
Lee, Y.J. (2007), "Assessment of tunnel collapse load by closed-form analytical solution and finite element analysis", *J. KGS*, **23**(4), 185-197.
Mazek, S.A. (2014), "Evaluation of surface displacement equation due to tunnelling in cohesionless soil", *Geomech*. *Eng*., *Int*. *J*., **7**(1), 55-73.
Sloan, S.W. and Assadi, A. (1993), "Stability of shallow tunnels in soft ground", *Proceedings of Wroth Memorial Symposium*, Predictive Soil Mechanics, Oxford, UK, July.
Wang, Z., Wong, R.C.K. and Heinz, H. (2010), "Assessment of long-term behaviour of a shallow tunnel in clay till", *Geomech*. *Eng*., *Int*. *J*., **2**(2), 107-123.
Yang, X.L. and Yan, R.M. (2015), "Collapse mechanism for deep tunnel subjected to seepage force in layered soils", *Geomech*. *Eng*., *Int*. *J*., **8**(5), 741-756.

JS

Appendix

Calculation of the upper bound for O+2

1. Work by pile working load (P_w) and soil self-weight (γ)

$$P_w = 144 \text{ kN/m}^2, \quad \gamma = 20 \text{ kN/m}^3, \quad L^* = 0.075 \text{ m}$$

*longitudinal length of soil container box in the model test

P_w & Blocks	Area (m^2)	W (kN)	ΔS (m)	$W \times \Delta S$ (kN-m)
P_w	0.0009375	0.1350000	0.0500	0.0067500
A	0.0003125	0.0004687	0.0500	0.0000234
B	0.0005228	0.0007842	0.0327	0.0000256
C	0.0008359	0.0012538	0.0910	0.0001141
D	0.0004649	0.0006974	0.1148	0.0000800
		Total		0.0069932

Note:
(1) Settlement (or displacement), ΔS of the pile is assumed to be 50 mm together with the block A.
(2) All the values of ΔS are corresponding to vertical displacements.

2. Work by tunnel: unknown value of P_0

P_0	L_T** (m)	L_T**×L* (m^2)	ΔS (m)	L_T**×L*×ΔS (m^3)
P_0D	0.0707107	0.0053033	0.0817	0.00043347
		Total		$0.00043347P_0$

**tunnel orthogonal length to P_0D's direction

3. UB (Upper Bound) solution

Work by pile working load (P_w) and soil self-weight (γ) = Work by tunnel: unknown value of P_0

$0.0069932 = 0.00043347P_0$
$P_0 = 16.133$ kPa